Research Article | Vol. 30, No. 8 / 11 Apr 2022 / Optics Express 12228
Optics EXPRESS

Narrow-bandwidth Bragg grating filter based on Ge-Sb-Se chalcogenide glasses

CHENFENG ZHOU,[1,2] XUELEI ZHANG,[1,2] YE LUO,[3,4] CHENG HOU,[1,2] ZHEN YANG,[1,2] WEI ZHANG,[1,2,*] LAN LI,[3,4] PEIPENG XU,[1,2] AND TIEFENG XU[5]

[1] *Faculty of Electrical Engineering and Computer Science, Ningbo University, Ningbo 315211, China*
[2] *Key Laboratory of Photoelectric Detecting Materials and Devices of Zhejiang Province, Ningbo 315211, China*
[3] *Key Laboratory of 3D Micro/Nano Fabrication and Characterization of Zhejiang Province, School of Engineering, Westlake University, 18 Shilongshan Road, Hangzhou 310024, China*
[4] *Institute of Advanced Technology, Westlake Institute for Advanced Study, 18 Shilongshan Road, Hangzhou 310024, China*
[5] *Ningbo Institute of Oceanography, Ningbo University, Ningbo 315211, China*
[*] *zhangwei3@nbu.edu.cn*

Abstract: Bragg grating (BG) filters play important roles in integrated photonics such as signal processing and optical sensing. In silicon-based counterpart photonic platforms, the application of narrow-bandwidth ($\Delta\lambda$) filters is often restrained by fabrication limitations. In this study, narrow-bandwidth BG filters based on Ge-Sb-Se chalcogenide materials are investigated. The structure of the filter is designed by optimizing the grating period, corrugation height, and grating number. The large corrugation of chalcogenide BG is more friendly and convenient for manufacturing process. The symmetric and asymmetric corrugation filters are then fabricated and characterized. Experimental results show a half-maximum bandwidth of 0.97 nm and 0.32 nm for symmetric and asymmetric filters, respectively, which demonstrates excellent narrow-bandwidth filtering performance of chalcogenide BG.

1. Introduction

Bragg gratings (BGs) are fundamental building blocks used in wide-ranging applications, such as optical communication [1,2], pulse shaping [3], photonic sensing [4,5], integrated microwave photonics [6,7] and narrow-linewidth lasers [8,9]. BG filters with narrow bandwidth are the subject of a long-term research direction, and significant efforts have been directed toward developing Bragg structures in planar waveguides [10–20].

In BG filters, spectral modulation can be achieved by varying the effective refractive index with different materials [21,22] or by modifying the grating geometry [15,16,18]. Over the past decade, many designed geometries, fabrication methods, and applications of BG devices on silicon-based materials have been investigated. The high-index contrast in silicon-based BGs exerts a much stronger modulation effect than that in normal waveguides. However, the achieved minimum grating corrugation is limited by the minimum feature size of the device. To obtain a bandwidth below 1 nm, the required minimum corrugation can be as small as 10 nm [23], which is a huge manufacturing challenge. To overcome this limitation, the use of chalcogenide glass (ChG) materials is promising [24,25]. ChGs have excellent properties, including wide infrared transparency window, flexible refractive index, integration ability onto different substrates without considering epitaxial lattice mismatch, and excellent infrared nonlinear optical performance. These features render them attractive for all-optical signal processing [26], chemical and biological sensing [27–29], and supercontinuum generation [30,31]. The reported applications of chalcogenide BGs include optical interconnection [32] and strong photoinduced

#450707 https://doi.org/10.1364/OE.450707
Journal © 2022 Received 8 Dec 2021; revised 7 Mar 2022; accepted 21 Mar 2022; published 28 Mar 2022

BGs [33] with As_2Se_3 or As_2S_3, but there are few relevant studies on ChG BG filters in recent years.

In this work, we propose and demonstrate an advanced BG filter by utilizing a high-index-contrast and nontoxic $Ge_{28}Sb_{12}Se_{60}$ (n = 2.72 @1550 nm) platform. Adjusting the structure parameters of the grating including grating period (Λ), corrugation height (ΔH), and number of the grating period (N) enables to obtain a narrow-bandwidth filter. Using electron beam lithography (EBL) exposure and plasma dry-etching technique, the high-quality narrowband symmetric and asymmetric ChG BG filters are successfully prepared. The minimum feature size reaches 160 nm, and the measured spectral bandwidth of the symmetric and asymmetric ChG BG filter is as narrow as about 0.97 nm and 0.32 nm, respectively. Compared with silicon-based counterparts, the relative smaller in refractive index in ChG enlarges the size of corrugation to ease the manufacturing difficulty, and provides better tolerance for manufacturing errors, while maintaining the narrow-band filtering effect. The research results demonstrate the feasibility of narrow-bandwidth BG filter for ChG, paving the way for applications in photonic filters and optical sensors.

2. Design of the BG filter

A BG filter has a periodic structure with modulation of the effective refractive index. Figure 1(a) shows the schematic of a uniform grating in a strip $Ge_{28}Sb_{12}Se_{60}$ waveguide using symmetric rectangular side-wall corrugations. Several important parameters including Λ, ΔH, and N are used to determine the performance of the filter. The structure design starts by selecting the width (W_{wg}) and height of the ChG waveguide using MODE Solution software for the simulation. The 3D view of the proposed ChG grating and the cross-section view of the electric field of the fundamental TE mode for the ChG waveguide are shown in Fig. 1(b), in which the height of the $Ge_{28}Sb_{12}Se_{60}$ waveguide is 300 nm. Figure 1(c) shows the effective indice at 1550 nm of TE_0, TM_0, and TE_1, TM_1 modes with different W_{wg} values. We can see that the width of the grating filter is usually greater than 350 nm to support a fundamental mode but less than 800 nm to avoid higher-order modes. The horizontal dotted line is the refraction index of the silicon oxide ($n = 1.44$), and the modes with refraction index greater than n_{SiO2} are guided [34]. Here, we focus on the TE mode operation because compared with the single-TM mode, the fundamental TE modes are strongly confined in the $Ge_{28}Sb_{12}Se_{60}$ layer core, which is conducive to achieving a narrow bandwidth. Meanwhile, too small size of the filter causes higher propagation loss due to the strong interaction with sidewall of the waveguide, so the W_{wg} of the filter waveguide is determined to be 600 nm.

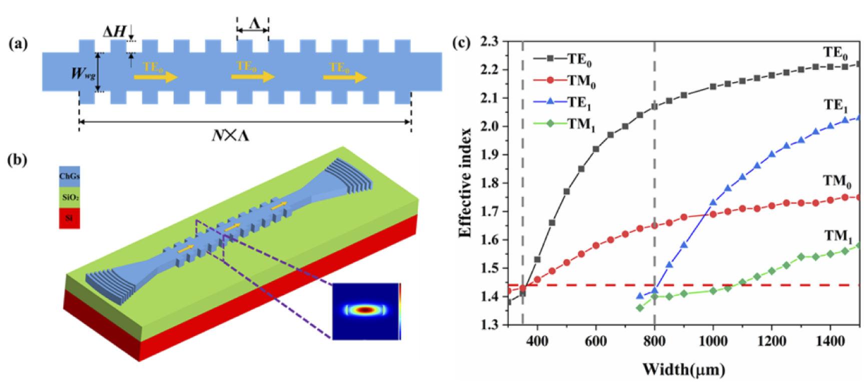

Fig. 1. (a) Top view of the BG. Λ is the grating period, ΔH is the corrugation height, and N is the number of the grating period. (b) Schematic of BG. (c) Effective indice at 1550 nm of the different TE/TM modes with the different ChG waveguide widths.

The incident light of the BG is reflected in a particular wavelength, named Bragg wavelength, and the grating period (Λ) is given as follows:

$$\lambda_B = 2\Lambda n_{eff}, \tag{1}$$

where n_{eff} is the effective index of the grating, λ_B is the Bragg wavelength of 1550 nm, and Λ can be calculated from the equation.

The bandwidth ($\Delta\lambda$) is a major figure of merit for the BG filter. From coupled-mode theory [35], the notch bandwidth can be theoretically estimated by:

$$\Delta\lambda = \frac{{\lambda_B}^2}{\pi n_g}\sqrt{\kappa^2 + \frac{\pi^2}{L^2}}, \tag{2}$$

where L is the length of the BG, κ is the coupling coefficient of the grating which can be explained by the amount of the reflection per unit length, and n_g is the group index. When the propagation constant deviation $\Delta\beta$=0, the rejection level (R) at the Bragg wavelength can be written as follows:

$$R = \tanh^2(\kappa L), \tag{3}$$

As shown in Eqs. (2) and (3), $\Delta\lambda$ and R are determined by κ and L, respectively. For a sufficiently long grating, $\Delta\lambda$ is primarily determined by κ. Thus, a nanoscale narrow-bandwidth filter requires a weak refractive-index modulation. In BG filters, ΔH is related to the refractive-index modulation [18], and the refractive-index modulation is commonly achieved by varying the refractive index or the waveguide characteristics. Conventional silicon-based Bragg narrowband grating filters require a 10 nm corrugation to accomplish a weak modulation due to the high-refractive-index contrast in the silicon platform. For ChGs, narrow bandwidth and generously robust rejection level can be determined by the grating parameters including N, ΔH, and Λ. Simulation results show that N has a huge impact on the rejection level, ΔH influences the bandwidth and the Bragg wavelength, and Λ affects the Bragg wavelength but has comparatively little effect on the transmission spectra. Through simulation, the optimal parameters are obtained as follows: $N = 1000$, $\Delta H = 160$ nm, and $\Lambda = 395$ nm.

Equation (3) clearly shows that R is proportional to L and $L = N\times\Lambda$, consistent with the traits shown in Fig. 2(a). Figure 2(a) also indicates that when N is larger than 1000, increasing N dose not enhance the rejection level of the grating filter. The manufacturing error of grating leads to intense propagation loss for large N, so $N = 1000$ is the trade-off between the manufacturing error and rejection level of the grating. ΔH determines κ, which greatly affects the filtering effect. Figure 2(b) shows the simulated transmission spectra for different ΔH values varying from 120 nm to 180 nm with 10 nm interval, indicating that the bandwidth initially decreases and then increases. The relative minimum bandwidth is found to reach 2 nm when ΔH is about 160 nm. The simulated spectra for the gratings of six different Λ values (380 nm to 405 nm with 5 nm interval) are plotted in Fig. 2(c), which shows the red-shifted Bragg wavelength with increased grating period and is coincident with Eq. (1). The optimal bandwidth can reach 0.81 nm, and the rejection level is 27 dB in the red dashed box, when N is 1000, ΔH is 160 nm, and Λ is 395 nm.

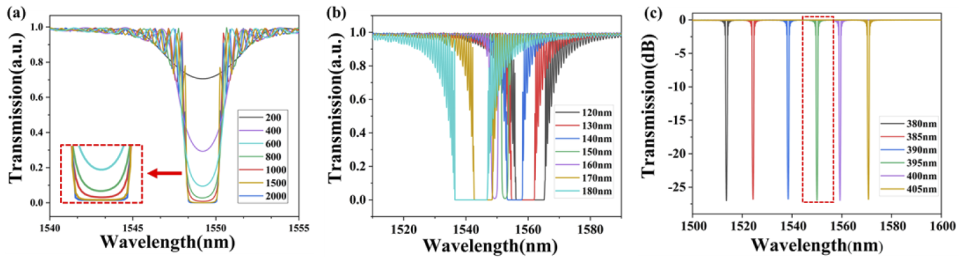

Fig. 2. (a) Simulated transmission spectra of ChG grating filter with various lengths ($L = N\times\Lambda$). Fixed parameters: $W_{wg} = 600$ nm, Λ=395 nm, and $\Delta H = 160$ nm. (b) Simulated transmission spectra of ChG gratings with different corrugation heights. Fixed parameters: W_{wg} =600 nm, Λ=395 nm, and $N = 1000$. (c) Simulated transmission spectra of ChG gratings with different grating periods. Fixed parameters: W_{wg} =600 nm, $\Delta H = 160$ nm, and $N = 1000$.

3. Fabrication of the BG filter

Based on the designed structure, an integrated chalcogenide-grating filter is fabricated using the following processes. The bottom substrate is a silicon wafer with a 2 µm-thick silicon dioxide layer, onto which a 300 nm-thick $Ge_{28}Sb_{12}Se_{60}$ film is thermally evaporated, followed by spin coating a 200 nm-thick positive ARP6200 photoresist. Then, the structure pattern is transferred using directing-writing 30kev EBL (Raith eLINE Plus). The etching process is explored with a gas mixture of CHF_3/CF_4 through inductively coupled plasma (ICP) etching (Oxford100), and parameters including gas-flow rate, chamber pressure, and radio frequency power are investigated (not shown here). Finally, the remaining photoresist is removed by oxygen-plasma cleaning with a gas mixture of $CHF_3/Ar/O_2$ before placing in N-methyl-2-pyrrolidone and heating on a hot plate.

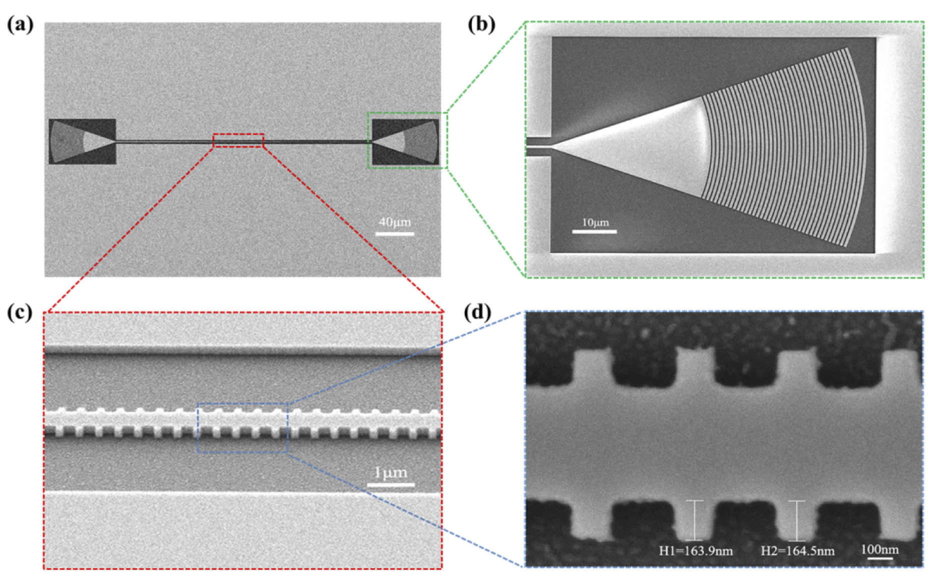

Fig. 3. (a) SEM image of GhG BG filter. (b) SEM image of the TE mode grating couple. (c) Details of the BG filter geometry. (d) Measurement of the corrugation heights: $H_1 = 163.9$ nm, $H_2 = 164.5$ nm.

Optics EXPRESS

Figure 3(a) shows the scanning electron microscopy (SEM) image of the chalcogenide BG filter. The fully etched fiber-waveguide grating coupler is depicted in Fig. 3(b). It facilitates the coupling light to the waveguide from an external fiber. The couplers achieve the optimal coupling effect with a duty cycle of 0.715 and a period of 920 nm through simulation. Figures 3(c) and 3(d) show the enlarged figures of the fabricated grating filter, the average value of the corrugation height is measured to be 160 nm ± 5 nm from multiple testing. The measurement results indicate that the fabrication offset of the corrugation is about 10 nm compared with the simulation results.

4. Performance of the BG filter

Figure 4(a) shows the schematic of the experimental setup. The system contains a continuous-wave tunable laser (Santac TSL-550) ranging from 1500 nm to 1630 nm. The light beam is coupled into the filter through a single-mode fiber (SMF), and the output light is collected to a low-noise power meter (Santec MPM210). Other auxiliary equipment includes the manual fiber polarization controllers (Thorlabs FPS526), which are used to maintain the polarization state of the fundamental TE mode light, and a CCD camera is used to monitor the position of the filter on the three-axis translation stage.

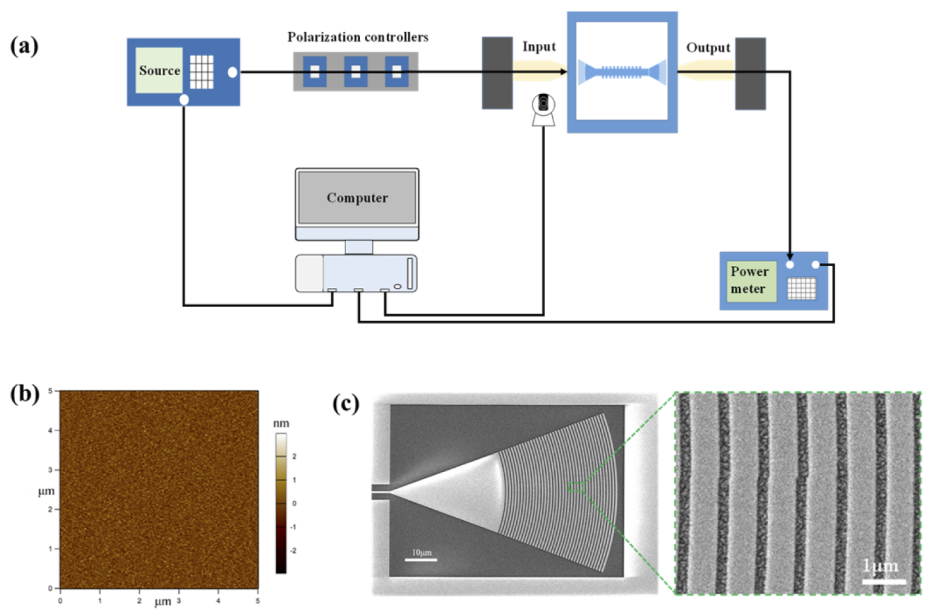

Fig. 4. (a) Schematic diagram of spectrum measurement experimental system. (b) AFM image of 300 nm Ge-Sb-Se film. (c) Stitching error of the chalcogenide grating coupler.

Equation (2) shows that as N increases, $\Delta\lambda$ should theoretically decreases. However, in experimental test, $\Delta\lambda$ broadens with increased grating length. The transmission spectra of the grating filter with different N values (500, 1000, 2000, and 5000) is shown in Fig. 5. We observe a slight decrease of power in the out-of-band transmission with increased N, which is caused by the increased propagation loss with increased grating length. The figure indicates that when N is 500, the transmission spectrum is clean, and when N is 1000, some irregular ripples are found. With increased N to 2000, the bandwidth remains approximately the same as that when $N = 1000$, and the transmission spectrum has some erratic ripples. When N reaches to 5000, the bandwidth increases and the noises become significant, which is far from the simulation. Firstly, we consider that the roughness of the Ge-Sb-Se film is the main reason why the simulated and measured spectra are different. After the surface roughness of the film has been measured

Optics EXPRESS

for several times by picking different areas using atomic force microscopy (AFM), the surface roughness is determined to be 0.347 nm (RMS), as shown in Fig. 4(b). Then, this assumption is disproved by the low surface roughness of the film.

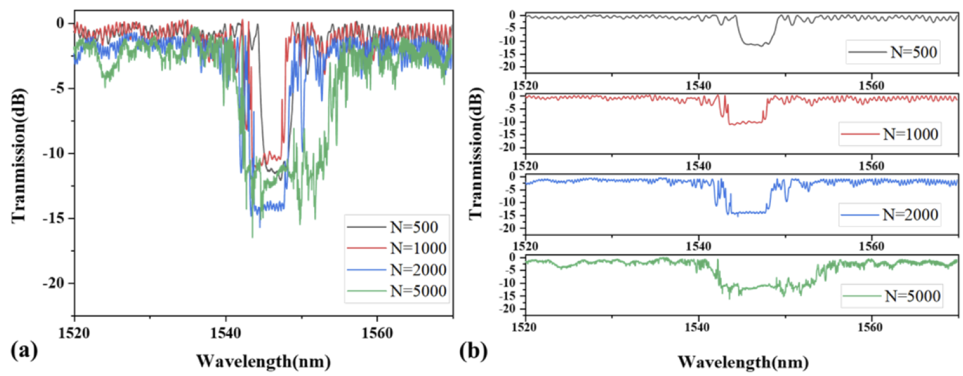

Fig. 5. (a) Measured transmission spectra for ChG BGs with different N values. Fixed parameters: W_{wg} =600 nm, Λ=395 nm, and ΔH =160 nm. (b) Details of the transmission spectra for different N values.

In fabrication process, 100 μm writing field is used to pattern the BG. The designed BG is much longer than 100 μm, and write field stitching is inevitable, which leads to the lateral and longitudinal offsets. The BG is sensitive to the continuity of the structure, and the stitching error has a negative impact on the performance of narrow-bandwidth BG filter [36]. Long BG will increase the times of write field stitches, which explain well why the bandwidth increases and the noises become significant when N reaches to 5000. The stitching errors are found in the chalcogenide grating coupler (shown in Fig. 4(c)) and BG parts by SEM image, and we assume that the stitching error is the main reason for the difference between the simulated and measured spectra.

According to theoretical analysis and simulation results, ΔH determines the coupling coefficient and the bandwidth. To prove the relation between ΔH and $\Delta\lambda$, and better understand the influence of different ΔH values on the spectra, a couple of grating filters with $N = 1000$ and different ΔH values ranging from 120 nm to 180 nm are fabricated (here, ΔH is the measured corrugation height). The measured transmission spectra are shown in Fig. 6. With increased ΔH, the transmission spectra are blue-shifted, and the experimental variation tendency of bandwidths is consistent with the simulation results shown in Fig. 2(b). The best filtering effect occurs when $\Delta H = 160$ nm.

Figure 7(a) shows the filtering effect of the symmetric BG filter based on the parameters discussed above, with a bandwidth of 0.97 nm and a rejection level of 24 dB, through Lorentz fitting. The narrow bandwidth below 1 nm is consistent with the previous simulation results. To further reduce the filter bandwidth while keeping the same feature size, the single-side asymmetric corrugation structure is implemented. With its characteristic size including Λ, ΔH, and N kept unchanged, this geometry halves the effective index different Δn_{eff} and consequently halves the coupling coefficient κ according to κ=$2\Delta n_{eff}/\lambda_B$. Based on Eqs. (2) and (3), the bandwidth and rejection level decrease with decreased κ. A single-side asymmetric BG filter is proposed, as shown in Fig. 7(b). It has a bandwidth of 0.32 nm, which shows that the asymmetric filter structure provides an evident bandwidth reduction compared with the regular filter geometry.

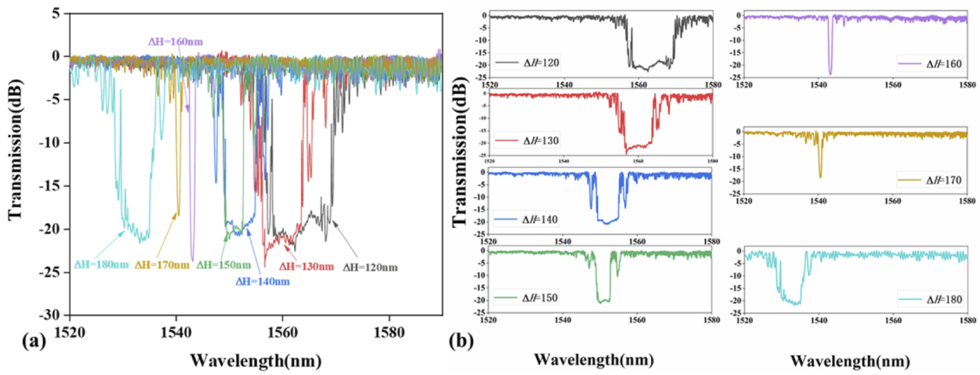

Fig. 6. (a) Measured transmission spectra for BGs with different ΔH values. Fixed parameters: W_{wg} =600 nm, Λ=395 nm, $N = 1000$. (b) Details of the transmission spectra for different ΔH values.

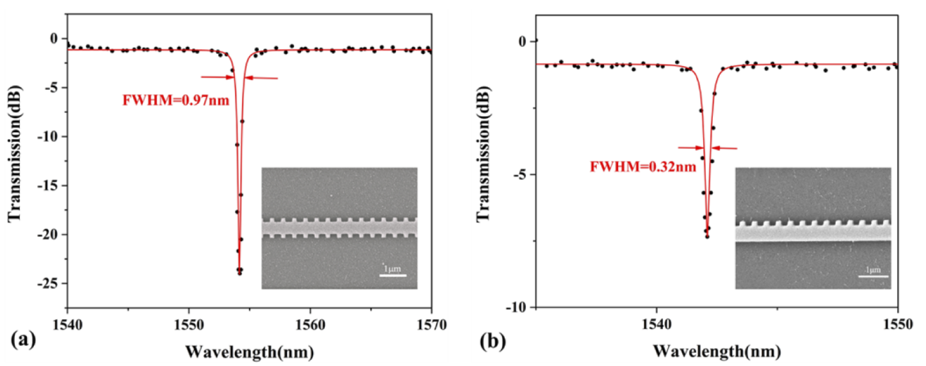

Fig. 7. (a) The Lorentzian fit to the resonance peak indicates a symmetric BG filter with a narrow bandwidth of 0.97 nm. The central wavelength of the symmetric BG is 1554 nm. (b) The Lorentzian fit to the resonance peak indicates an asymmetric BG filter with a narrow bandwidth of 0.32 nm. The central wavelength of the asymmetric BG is 1542 nm.

5. Conclusion

In conclusion, we propose and experimentally demonstrate a ChG BG filter. The ChG platform could maintain the narrow-band filtering effect while providing better tolerance for manufacturing errors. To obtain a narrow bandwidth, the optimal parameters of the BG filter are investigated through simulation. With a minimum feature size of 160 nm in the capabilities of EBL, the BG filter is fabricated through a single-etch step process, and the manufacturing error of the corrugation is below 10 nm. The symmetric BG filter shows a bandwidth of 0.97 nm with a strength of 24 dB, and the single-side asymmetric BG filter demonstrates better narrow-bandwidth filtering performance with a bandwidth of 0.32 nm. The combination of the refractive-index flexibility of ChGs and the structure-design diversity of BG filter enables the application of ChGs in high-performance narrowband filters for integrated photonics.

Funding. Natural Science Foundation of Zhejiang Province (LD19F050001, LD22F040002); National Natural Science Foundation of China (12104375, 61875099, 62175202); K. C. Wong Magna Fund in Ningbo University.

Disclosures. The authors declare no conflicts of interest.

Data availability. Data underlying the results presented in this paper are not publicly available at this time but may be obtained from the authors upon reasonable request.

References

1. K. Ikeda, R. Konoike, K. Suzuki, and H. Kawashima, "2 × 2 16-ch silicon photonics wavelength-selective switch based on waveguide gratings," Opt. Express **28**(18), 26861–26869 (2020).
2. L. R. Chen, J. Wang, B. Naghdi, and I. Glesk, "Subwavelength Grating Waveguide Devices for Telecommunications Applications," IEEE J. Sel. Top. Quantum Electron **25**(3), 1–11 (2019).
3. K. T. Crampton, A. G. Joly, and P. Z. El-Khoury, "Surface plasmon polariton pulse shaping via two-dimensional Bragg grating pairs," Nanophotonics **10**(2), 959–965 (2020).
4. C. Perez-Armenta, A. Ortega-Monux, J. Ctyroky, P. Cheben, J. H. Schmid, R. Halir, I. Molina-Fernandez, and J. G. Wanguemert-Perez, "Narrowband Bragg filters based on subwavelength grating waveguides for silicon photonic sensing," Opt. Express **28**(25), 37971–37985 (2020).
5. E. Luan, H. Shoman, D. M. Ratner, K. C. Cheung, and L. Chrostowski, "Silicon Photonic Biosensors Using Label-Free Detection," Sensors **18**(10), 3519 (2018).
6. I. Giuntoni, D. Stolarek, D. I. Kroushkov, J. Bruns, L. Zimmermann, B. Tillack, and K. Petermann, "Continuously tunable delay line based on SOI tapered Bragg gratings," Opt. Express **20**(10), 11241–11246 (2012).
7. W. Zhang and J. Yao, "Silicon-Based Integrated Microwave Photonics," IEEE J. Quantum Electron. **52**(1), 1–12 (2016).
8. A. Congar, M. Gay, G. Perin, D. Mammez, J. C. Simon, P. Besnard, J. Rouvillain, T. Georges, L. Lablonde, T. Robin, and S. Trebaol, "Narrow linewidth near-UV InGaN laser diode based on external cavity fiber Bragg grating," Opt. Lett. **46**(5), 1077–1080 (2021).
9. M. Henriksson, L. Sjöqvist, V. Pasiskevicius, and F. Laurell, "Narrow linewidth 2 μm optical parametric oscillation in periodically poled LiNbO3 with volume Bragg grating outcoupler," Appl. Phys. B **86**(3), 497–501 (2007).
10. D. Oser, F. Mazeas, X. Le Roux, D. Pérez-Galacho, O. Alibart, S. Tanzilli, L. Labonté, D. Marris-Morini, L. Vivien, É. Cassan, and C. Alonso-Ramos, "Coherency-Broken Bragg Filters: Overcoming On-Chip Rejection Limitations," Laser Photonics Rev. **13**(8), 1800226 (2019).
11. T. Sharma, V. Rana, J. Wang, Z. Cheng, Y. Chen, Y. Geng, X. Hong, X. Li, K. Yu, and B. K. Kaushik, "Design of grating based narrow band reflector on SOI waveguide," Optik **227**, 165995 (2021).
12. Y. Yao, H. Liu, L. Xue, B. Liu, and H. Zhang, "Design of lithium niobate phase-shifted Bragg grating for electro-optically tunable ultra-narrow bandwidth filtering," Appl. Opt. **58**(25), 6770–6774 (2019).
13. D. Mu, H. Qiu, J. Jiang, X. Wang, Z. Fu, Y. Wang, X. Jiang, H. Yu, and J. Yang, "A Four-Channel DWDM Tunable Add/Drop Demultiplexer Based on Silicon Waveguide Bragg Gratings," IEEE Photonics J. **11**(1), 8 (2019).
14. D. T. Spencer, M. Davenport, S. Srinivasan, J. Khurgin, P. A. Morton, and J. E. Bowers, "Low kappa, narrow bandwidth Si(3)N(4) Bragg gratings," Opt. Express **23**(23), 30329–30336 (2015).
15. H. Qiu, L. Lin, P. Yu, T. Dai, X. Jiang, and H. Yu, "Narrow-Band Add-Drop Filter Based on Cladding-Modulated Apodized Multimode Bragg Grating," J. Lightwave Technol. **37**(21), 5542–5547 (2019).
16. T. Yen and Y. Hung, "Narrowband Dual-Wavelength Silicon Waveguide Bragg Reflectors," J. Lightwave Technol. **37**(20), 5326–5332 (2019).
17. X. Wang, W. Shi, H. Yun, S. Grist, N. A. F. Jaeger, and L. Chrostowski, "Narrow-band waveguide Bragg gratings on SOI wafers with CMOS-compatible fabrication process," Opt. Express **20**(14), 15547–15558 (2012).
18. D. Oser, D. Perez-Galacho, X. Le Roux, S. Tanzilli, L. Vivien, L. Labonte, E. Cassan, and C. Alonso-Ramos, "Silicon subwavelength modal Bragg grating filters with narrow bandwidth and high optical rejection," Opt. Lett. **45**(20), 5784–5787 (2020).
19. D. Oser, D. Perez-Galacho, C. Alonso-Ramos, X. Le Roux, S. Tanzilli, L. Vivien, L. Labonte, and E. Cassan, "Subwavelength engineering and asymmetry: two efficient tools for sub-nanometer-bandwidth silicon Bragg filters," Opt. Lett. **43**(14), 3208–3211 (2018).
20. I. Giuntoni, A. Gajda, M. Krause, R. Steingrüber, J. Bruns, and K. Petermann, "Tunable Bragg reflectors on silicon-on-insulator rib waveguides," Opt. Express **17**(21), 18518–18524 (2009).
21. E. Durán-Valdeiglesias, S. Guerber, D. Oser, X. Le Roux, D. Benedikovic, D. Pérez-Galacho, N. Vulliet, S. Cremer, S. Monfray, and E. Cassan, "Dual-polarization silicon nitride Bragg filters with low thermal sensitivity," Opt. Lett. **44**(18), 4578–4581 (2019).
22. K. Abdelsalam, E. Ordouie, M. G. Vazimali, F. A. Juneghani, P. Kumar, G. S. Kanter, and S. Fathpour, "Tunable dual-channel ultra-narrowband Bragg grating filter on thin-film lithium niobate," Opt. Lett. **46**(11), 2730–2733 (2021).
23. X. Wang, W. Shi, R. Vafaei, N. A. F. Jaeger, and L. Chrostowski, "Uniform and Sampled Bragg Gratings in SOI Strip Waveguides with Sidewall Corrugations," IEEE Photonics Technol. Lett. **23**(5), 290–292 (2011).
24. C. R. Schardt, J. H. Simmons, P. Lucas, L. Le Neindre, and J. Lucas, "Photodarkening in Ge_3Se_{17} glass," J. non-cryst. Solids **274**(1-3), 23–29 (2000).
25. B. Bureau, X. H. Zhang, F. Smektala, J.-L. Adam, J. Troles, H.-L. Ma, C. Boussard-Plèdel, J. Lucas, P. Lucas, D. Le Coq, M. R. Riley, and J. H. Simmons, "Recent advances in chalcogenide glasses," J. Non-Cryst. Solids **345-346**, 276–283 (2004).
26. E. Yousefi and M. Hatami, "All optical self signal processing using chalcogenide nonlinear fiber Bragg grating," Optik **125**(22), 6637–6640 (2014).
27. W. Huang, Y. Luo, W. Zhang, C. Li, L. Li, Z. Yang, and P. Xu, "High-sensitivity refractive index sensor based on Ge–Sb–Se chalcogenide microring resonator," Infrared Phys. Techn. **116**, 103792 (2021).

Optics EXPRESS

28. Z. Yang, R. Zhang, Z. Wang, P. Xu, W. Zhang, Z. Kang, J. Zheng, S. Dai, R. Wang, and A. Majumdar, "High-Q, submicron-confined chalcogenide microring resonators," Opt. Express **29**(21), 33225–33233 (2021).
29. R. Zhang, Z. Yang, M. Zhao, P. Xu, W. Zhang, Z. Kang, J. Zheng, S. Dai, R. Wang, and A. Majumdar, "High quality, high index-contrast chalcogenide microdisk resonators," Opt. Express **29**(12), 17775–17783 (2021).
30. Y. Yu, X. Gai, P. Ma, K. Vu, Z. Yang, R. Wang, D. Y. Choi, S. Madden, and B. Luther-Davies, "Experimental demonstration of linearly polarized 2-10 µm supercontinuum generation in a chalcogenide rib waveguide," Opt. Lett. **41**(5), 958–961 (2016).
31. J. Hwang, D. G. Kim, S. Han, D. Jeong, Y. H. Lee, D. Y. Choi, and H. Lee, "Supercontinuum generation in As2S3 waveguides fabricated without direct etching," Opt. Lett. **46**(10), 2413–2416 (2021).
32. W. Shen, P. Zeng, Z. Yang, D. Xia, J. Du, B. Zhang, K. Xu, Z. He, and Z. Li, "Chalcogenide glass photonic integration for improved 2-micron optical interconnection," Photonics Res. **8**(9), 1484–1490 (2020).
33. T. G. Robinson, R. G. DeCorby, J. N. McMullin, C. J. Haugen, S. O. Kasap, and D. Tonchev, "Strong Bragg gratings photoinduced by 633-nm illumination in evaporated As_2Se_3 thin films," Opt. Lett. **28**(6), 459–461 (2003).
34. A. S. Bonnet, G. Caloz, and F. Mahé, "Guided modes of integrated optical guides. A mathematical study," J. App. Maths **60**(3), 225–261 (1998).
35. W.-P. Huang and J. Mu, "Complex coupled-mode theory for optical waveguides," Opt. Express **17**(21), 19134–19152 (2009).
36. S. Zamek, M. Khajavikhan, D. T. Tan, M. Ayache, B. Slutsky, and Y. Fainman, "Effects of lithographic stitching errors on the performance of waveguide Bragg gratings," arXiv:1110.6867v1 [physics.optics] (2011).